9150-873

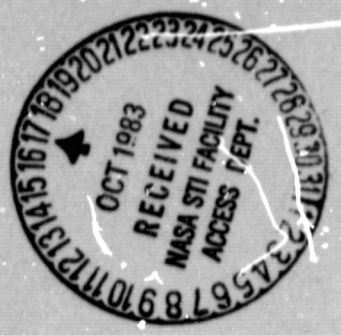

DOE/JPL-956289-83/1
Dist.Category UC-63

STUDY OF RELATIONSHIPS OF MATERIAL PROPERTIES AND HIGH EFFICIENCY SOLAR CELL PERFORMANCE ON MATERIAL COMPOSITION

FIRST TECHNICAL REPORT

July 1983

By C. T. Sah

Contract No. 956289

The JPL Flat-Plate Solar Array (FSA) Project is sponsored by the U. S. Department of Energy (DOE) and forms part of the Photovoltaic Energy Systems Program to initiate a major effort toward the development of cost-competitive solar arrays. This work was performed for the Jet Propulsion Laboratory, California Institute of Technology, and the Department of Energy, through an agreement between the National Aeronautics and Space Administration and the Department of Energy.

DOE/JPL-956289-83/1
Dist.Category UC-63

STUDY OF RELATIONSHIPS OF MATERIAL PROPERTIES AND HIGH EFFICIENCY SOLAR CELL PERFORMANCE ON MATERIAL COMPOSITION

FIRST TECHNICAL REPORT

July 1983

By C. T. Sah

Contract No. 956289

The JPL Flat-Plate Solar Array (FSA) Project is sponsored by the U. S. Department of Energy (DOE) and forms part of the Photovoltaic Energy Systems Program to initiate a major effort toward the development of cost-competitive solar arrays. This work was performed for the Jet Propulsion Laboratory, California Institute of Technology, and the Department of Energy, through an agreement between the National Aeronautics and Space Administration and the Department of Energy.

TECHNICAL CONTENT STATEMENT

NEW TECHNOLOGY

No new technology is reportable for the period covered by this report.

TABLE OF CONTENT

LIST OF ILLUSTRATION

LIST OF TABLE

There is no table in this technical report.

PREFACE

The objectives of this program are generally described by the title of its contract support, Study of Relationships of Material Properties and High Efficiency Solar Cell Performance on Material Composition. There are two interrelated tasks: (1) theoretical and experimental studies of impurity related energy levels, densities of these levels and electron and hole thermal capture and emission rates at these levels; and (2) generation of mathematical models to describe the experimental results and to specify the material properties and device structures required for very-high-efficiency solar cells.

The main effort on task 1 has dealt with accurate measurements of the thermal capture and emission rates of electrons and holes at the recombination centers from residual impurities in high-efficiency solar-cell grade silicon. Experiments are performed on silicon single crystals intentionally doped with selected transition metal impurities, such as Ti. In order to measure very large capture rates of both majority and minority carriers at these impurity recombination centers, refinements and careful implementation of the various capacitance and current transient methods, proposed and demonstrated by this author and his graduate students during 1966-1970, have been undertaken using automated data acquisition system under the complete control of minicomputer systems. At present, the four thermal capture rates and the two majority carrier thermal emission rates at the two energy levels of the double-donor Ti impurity have been accurately determined over a wide range of temperatures above 77K. Analyses for optimum cell design will be undertaken and reported shortly.

Task 2 has been concerned with a search of cell geometries and material characteristics to achieve very high efficiency and to delineate the causes which limit the performance. This report contains the results of detailed and extensive theoretical and numerical analyses of the anticipated performance enhancement from deep penetrating back-surface-field layer. It was demonstrated in previous and published work that short-circuiting defects across the back-surface-field layer can seriously reduce the open-circuit voltage and conversion efficiency. Their pernicious effects should be reduced if the back-surface-field layer is thickened from the traditional one to five microns to tens of microns, since a thick layer is less likely to be penetrated and hence short-circuited by a surface defect on the back surface than a thin layer. The main conclusion from the numerical analyses of about 100 cells is that for the optimum thickness cell at 50 micron total thickness, the back-surface-field layer should be more than 20 micron thick in order to obtain the high open-circuit voltage. For a thicker BSF layer, the open-circuit voltage would level off to about 710 mV, the short-circuit current to about 30 mA/cm^2, and the AM1 efficiency to 20%. These values are now limited by Auger recombination in the diffused emitter while base recombination has rather little effect even the carrier lifetimes in the base are only 20 us. Thus, with an extended back surface field or back drift field, additional performance improvement can be realized only through emitter design to reduce emitter recombination from the various sources, such as Auger recombination and energy gap narrowing due to high dopant impurity concentrations. Analyses for optimum emitter design are planned which will take into account of the cell structures under investigation by the JPL and SERI basic understanding projects.

ABSTRACT

This paper analyzes the performance improvements obtainable from extending the traditionally thin back-surface-field (BSF) layer deep into the base of silicon solar cells under terrestrial solar illumination (AM1). This extended BSF cell is also known as the back-drift-field cell. About 100 silicon cells have been analyzed, each with a different emitter or base dopant impurity distribution whose selection was based on physically anticipated improvements. The four principal performance parameters (the open-circuit voltage, the short-circuit current, the fill factor, and the maximum efficiency) are computed using a FORTRAN program, called Circuit Technique for Semiconductor-device Analysis, CTSA, which numerically solves the six Shockley Equations under AM1 solar illumination at 88.92 mW/cm^2, at an optimum cell thickness of 50 um. The results show that very significant performance improvements can be realized by extending the BSF layer thickness from 2 um (18% efficiency) to 40 um (20% efficiency). The immunity of cell performance to recombination defect or impurity center is also improved by a factor of two to three in the recombination center density. For 20% p+/n/n+ cells with about 20 us base lifetime, a 20 um BSF penetration is sufficient. At this or deeper penetrations, interband Auger recombination in the emitter layer becomes the limiting factor and affects mainly the short-circuit current but not the open-circuit voltage which has saturated to about 710 mV.

PERFORMANCE IMPROVEMENTS FROM PENETRATING BACK SURFACE FIELD IN VERY HIGH EFFICIENCY TERRESTRIAL THIN FILM CRYSTALLINE SILICON SOLAR CELL

I. INTRODUCTION

Back-surface-field (BSF) solar cell is a semiconductor junction device that contains a high-low junction or a high-majority-carrier-density layer on the back surface (p base/p+ layer or n base/n+ layer). The potential barrier at the BSF high-low junction prevents the minority carriers from reaching the back surface of the semiconductor which usually has a very high surface recombination velocity since it is usually covered with a metal layer to provide a low resistance ohmic contact. This barrier greatly reduces the total base recombination current, resulting in a substantial increase of the open-circuit voltage over a comparable cell that has no back-surface-field layer [1].

The traditional back-surface-field layer is quite thin, about one to five microns. Its thickness is limited by its formation technology, such as aluminum diffusion during alloying to form the p/p+ low-high junction as well as the ohmic contact [1], or by dopant impurity diffusion from a vapor source to form either the p/p+ or the n/n+ BSF junction in recent high-efficiency cell designs [2]. In both cases, the thinness is a result of the low diffusivity of dopant impurity at the relatively low processing temperatures, about 800C for aluminum alloying and 1000C for boron or phosphorus diffusion. The low diffusion temperature was necesasry to maintain a high minority carrier lifetime and hence low recombination rate in the base layer.

It has been demonstrated by us [3,4] that random defects across the thin back-surface-field layer can greatly reduce the open-circuit voltage of a high-efficiency BSF solar cell, if the defect is an electrical short circuit or has a low electrical resistance. The deleterious effects of a short-circuit defect across the BSF layer on the circumference or edge of a cell can be reduced by increasing the cell area [3]. However, the presence of even a few (even one) short-circuiting defect across the BSF layer in the interior or away from the perimeter of the cell can give a large reduction of the open circuit voltage [4].

The current state-of-the-art for reaching very high efficiency has been centered on exploring ways to increase the open-circuit voltage [5-8] since the short-circuit current has reached values to within about 10% of the highest achievable value while there is still room for 20% or more improvement in open-circuit voltage. A significant improvement of the open-circuit voltage can be realized by reducing the total cell thickness of a BSF cell since this reduces the active recombination volume confined by the back-surface-field low-high junction. Computer-aided-analysis (CAA) was used to demonstrate that for a thin-BSF-layer cell, its AM1 efficiency peaks at a cell thickness of about 50 um [9].

In the above thin-BSF-layer cell structures, open-circuit voltage degradation from defects across the BSF layer can be quite serious in a practical manufacturing technology since the cell area is very large and the presence of even just one defect can be very degrading. Simple geometrical considerations immediately suggest that if the BSF layer is made very thick or deeply penetrating or extended into the base layer of a cell, then there is less likelihood of short-circuiting by defects if the defects are shallow surface defects on the back surface of the cell.

In addition to higher immunity from short-circuiting bulk defects, a thick back-surface-field layer, penetrating deeply into and extended over a major portion of the base region, can further increase the open-circuit voltage since the base recombination volume is decreased. Furthermore, the built-in electric field extended over the entire base layer, from the thick penetrating back-surface-field layer, should also improve the collection efficiency or help the separation of the photo-generated electron-hole pairs before they recombine, thereby improving the short-circuit current. This latter improvement would diminish at high solar concentration or high injection level since the built-in electric field from the dopant impurity density gradient would be wiped out by the high densities of electrons and holes. As a consequence of the built-in electric field, the extended BSF cell is also known as the back-drift-field (BDF) solar cell.

The purpose of this paper is to employ exact numerical analyses to determine the effects of extended back-surface fields from which some optimum device designs are suggested and the residual basic mechanisms, which limit further performance improvement, are delineated.

The effect of the penetration depth on the cell performance is demonstrated in section II. In section III, improvements in immunity to the presence of recombination centers in the base are illustrated and quantitatively evaluated. In section IV, the origin of the differences between the n+/p/p+ and p+/n/n+ cells is delineated which is further illustrated by the 'local' steady-state lifetime variation in the emitter described in section V. These lead to a demonstration of the importance of emitter recombination as the limiting factor for further improvement of the cell performance. Conclusion and summary are given in section VI.

II. EFFECTS OF BACK-SURFACE-FIELD PENETRATION

Previous analyses of thin-BSF-layer cells indicated that the optimum cell thickness for maximum efficiency is around 50 um [9]. Below 50 um, the open-circuit voltage continues to increase but the short-circuit current decreases more rapidly, giving rise to an efficiency maximum. However, the efficiency peak is fairly broad, covering nearly a two-to-one range of thickness. Thus, in this analysis, a total cell thickness of 50 um is selected to illustrate the further performance improvements realizable from the extension of the BSF layer.

The numerical analysis technique has been described previously [10]. The Shockley (or Semiconductor) Equations, in this case seven coupled nonlinear one-dimensional differential equations for a two-level-recombination-center model, are numerically solved by a sythesized circuit technique (SCT) coded in a FORTRAN program called Circuit Technique for Semiconductor-device (or Solar-cell) Analysis (CTSA). The small-signal-error and the d.c. equivalent-circuit models, in the form of two three-wire, one-dimensional, and lumped-section transmission lines, are first synthesized from the seven Shockley Equations. The thickness of the cell is divided into 198 sections, giving 198 lumped sections for each of the two transmission lines. Both ends of the transmission lines are short-circuited to simulate the infinite surface or interface recombination conditions. Finite interface recombination velocities were also tested giving no difference in results as expected since Auger recombination rates at the two degenerately doped surfaces are exceedingly high which overshadow any interface recombination velocity variation from non-Auger recombination processes, such as the Shockley-Read-Hall thermal recombination processes. The variation of the thickness of the 198 lump sections, known as a

'computer model', is selected to provide physically estimated best-accuracy and fast convergent numerical solutions. The computer model divides the cell into four layers, the quasi-neutral emitter, the space-charge, the quasi-neutral base, and the BSF layers. For the base doping of 1.0E17 cm^{-3},# the number of lumped sections in the four layers are: 22, 60, 91 and 25 respectively, which will be known as the 22/60/91/25 computer model. Special nonuniform variations of the thickness of each lump section are also employed so that the adjacent lump sections do not differ by more than three in thicknesses. For the 5.0E15 cm^{-3} substrate impurity doping, a computer model of 25/50/123 is used for thicker than 20 um BSF layers and a 25/50/73/50 model is used for shallower BSF layers. Judicious choices of the computer model, based on physical reasoning, must be made to give accurate and fast convergent numerical solutions. Accurate and real AM1 solar spectrum [10] is employed with a total power of 88.92 mW/cm^2 instead of the 100 mW/cm^2 AM1.5 used in laboratory tests. Thus, the short-circuit current in laboratory tests is 100/88.92=1.1246 times higher or 12.46% higher than that obtainable on earth surface at high noon. In addition, we assumed no reflection loss at the front surface and complete transmission at the back surface, i.e., one optical pass. In realistic situation, the back surface will reflect the unabsorbed light to approach a two optical-path situation but the increase of the short-circuit current is not large as we have demonstrated [9]. The analysis is carried out at an intrinsic carrier density of 1.0E10 cm^{-3} which corresponds to a device temperature of 297.15K. At a realistic and somewhat higher device operating temperature of 34C, or 10C higher than assumed, the open-circuit voltage will drop as -3T*log(T) due to the increase of the effective density-of-states with temperature and our

The notation used in this paper follows the FORTRAN convention. E17 is 10^{17}.

results can be appropriately scaled. The other material constants such as mobilities, effective masses, interband Auger recombination rates, thermal capture and emission rates (double-acceptor zinc recombination model), and energy gap narrowing due to Debye screening are similar to those used in previous analyses [9,10]. The BSF dopant impurity profile is assumed to be exponential to simulate a constant drift or built-in electric field. Although a more realistic profile can be readily used but it gives the same conclusions. Variation of the emitter diffusion profile is made to explore the effect of Auger recombination. This is presented in Section IV.

The p+/n/n+ extended BSF cells are analyzed to determine the optimum penetration of the BSF layer. The impurity density profile used is given by

$$N_{AA} - N_{DD} = C_0[1 - (x/L_1)^{2/3}] - C_B - C_L\exp[-(L-x)/L_2] \qquad (1)$$

where C_0=2.5E20, C_B=1.0E17 or 5.0E15, C_L=5.0E18, L=50 um, L_1 is determined by the front junction depth of X_J=0.25 um, while L_2 is determined by the BSF penetration depth whose values are 1, 2, 5, 10, 15, 20, 25, 30, 40, 45, 48 um and other in-between values. The emitter diffusion profile given above comes from an empirical fit of the experimentally measured boron diffusion profile which was used previously [10]. It will be shown in Sections IV and V that when base recombination is reduced by the extension of the BSF layer and emitter recombination is the limiting factor, the emitter dopant impurity profile will determine the limiting efficiency through the short-circuit current due to interband Auger recombination in the degenerate emitter.

The numerical results of the open-circuit voltage, VOC, the short-circuit current density, JSC, the fill factor, FF, and the maximum efficiency, EFF, at AM1 solar illumination are given in Fig. 1 for the low-base-resistivity cell with CB=1.0E17 cm^{-3}.

The general trend is clearly evident. The VOC increases with BSF penetration depth, but the major rise occurs in the penetration range from 0 to about 20 um. For deeper penetration, the gain in VOC becomes smaller, eventually saturating to about 710 mV.

The major increase of JSC also occurs in the penetration range of 0 to 20 um, reaching a maximum of about 30 mA/cm^2 at about 20 um. Deeper penetration actually reduces JSC because of the increased Auger recombination volume in the highly doped base. The display of this fine-grain variation is a feature of the accurate and exact numerical analyses which cannot be obtained from simple and approximate analytical solutions.

The fill factor (FF) variation with BSF penetration shown in Fig. 1 is rather uneventful since it is a relatively weak function of the open-circuit voltage, VOC. However, the high value of nearly 0.85 indicates that the cell approaches the ideal Shockley diode law.

The combined VOC and JSC variations give an efficiency variation with BSF penetration depth that has a very rapid initial rise in the range of 0 to 20 um penetration since both VOC and JSC increase rapidly in this range. The efficiency saturates to about 20% when the BSF penetration is deeper than about 20 um. The saturation is the result of increasing VOC and decreasing JSC, caused by Auger recombination in the BSF layer, with deeper BSF penetration.

Thus, for such a low-resistivity (CB=1.0E17cm^{-3}), optimum-thickness (50 um), and 20-us-base-lifetime cell, significant performance gains are realized when the BSF penetration is deeper than about 20 um. In

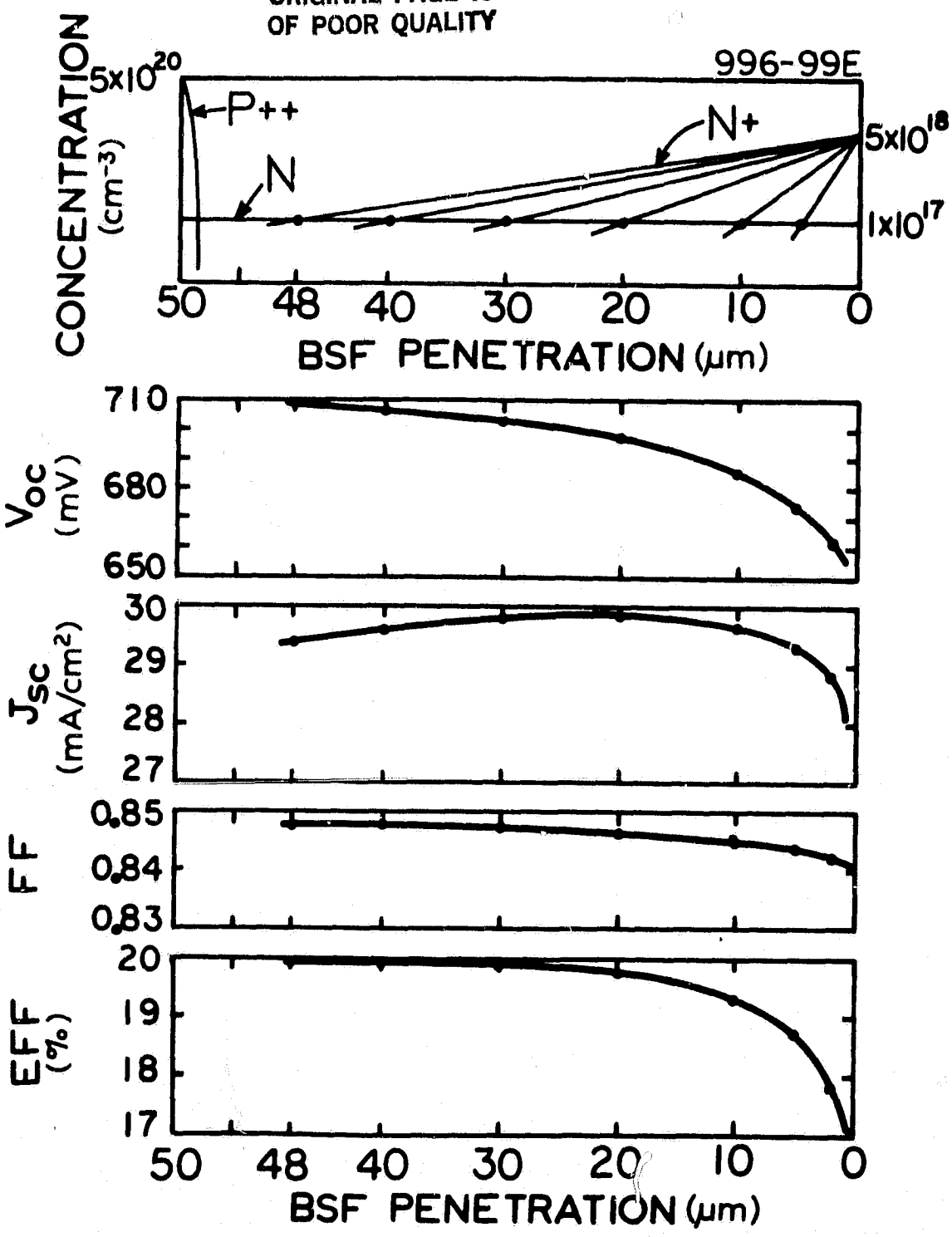

Fig. 1. Effect of BSF penetration on the performance of p+/n/n+ silicon solar cells with base dopant density of 1.0E17 cm^{-3}.

practice, a deeper penetration may be desirable for both low cost, such as an thin epitaxial layer grown on a very-low-resistivity substrate at a high temperature for a short time so as to rely on the outdiffusion of the substrate impurity into the epitaxial film, and for high immunity to short-circuiting bulk defects. It is evident from Fig. 1 that even for a 2 um epitaxial film or 48 micron BSF penetration, the efficiency is still maintained at about the maximum, 20%.

At the maximum or 20% efficiency, the limiting factor is no longer base recombination; but instead, emitter recombination plays the dominant role. Thus, the 20% plateau can be raised by proper emitter design. In Section IV, the importance of emitter recombination will be demonstrated.

The effects on cell performance from BSF penetration depth are also analyzed for a high-base-resistivity-cell family with a base dopant density of CB=5.0E15 cm^{-3}. The results are given in Fig. 2.

It is evident that the BSF penetration has a large effect on the VOC since the base doping is lower so that VOC is more dependent on the total majority carrier density in the BSF layer than that in a lower base resistivity or higher base-carrier-density cell. At 48 um, VOC has not saturated, but it would saturate to the 710 mV level of the 1.0E17 cm^{-3} cell of Fig. 1 when the BSF impurity density penetrates further to raise the overall n-type impurity or electron density in the remaining 2 um layer to 1.0E17 cm^{-3} level.

The JSC saturates to about 30.5 mA/cm^2 and is nearly flat over a wide range of BSF penetration. Its value is somewhat higher than the low-resistivity cell mainly from a slightly higher base lifetime of about 25 us versus the 20 us obtained for the low-resistivity cell.

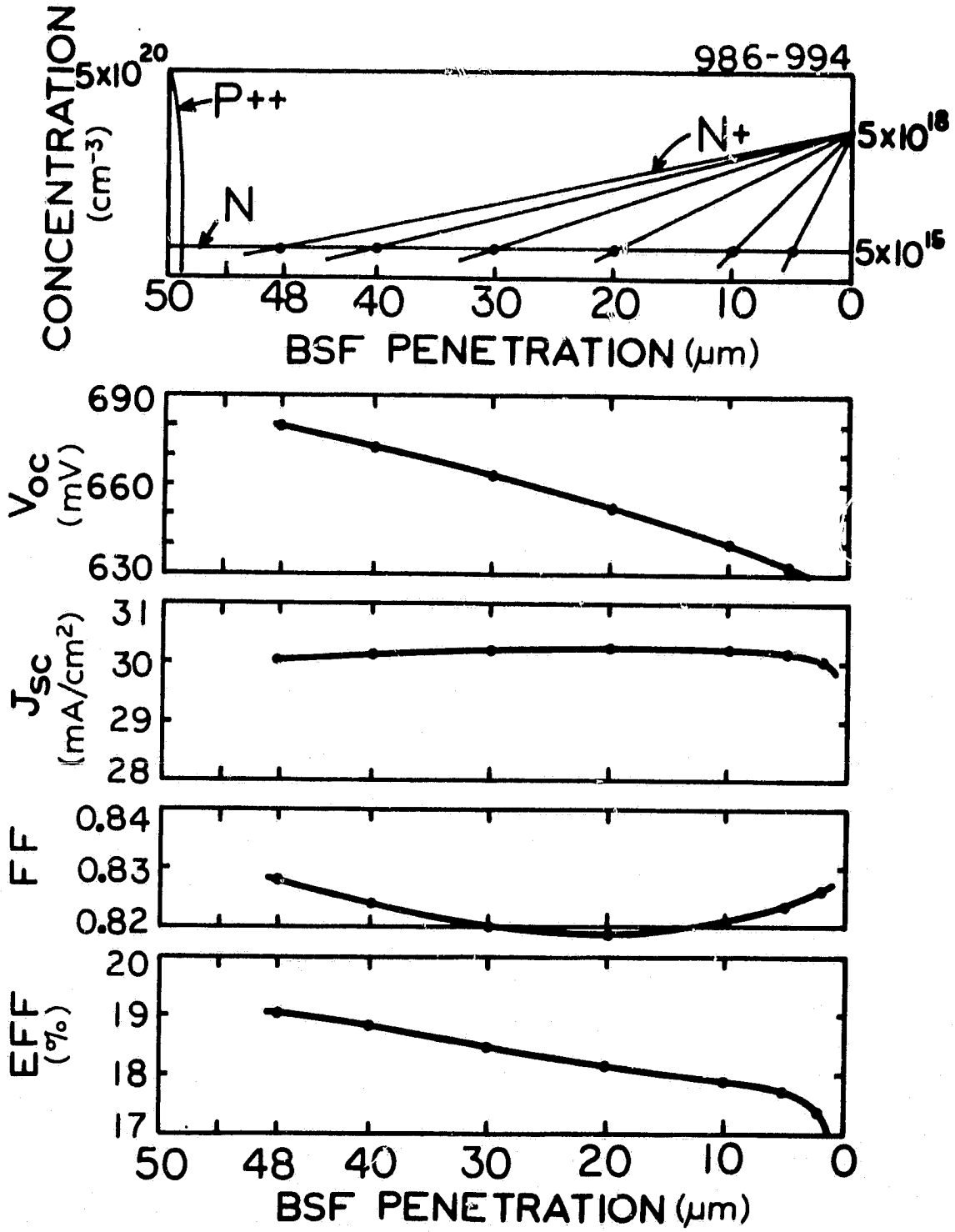

Fig. 2. Effect of BSF penetration on the performance of p+/n/n+ silicon solar cells with base dopant density of 5.0E15 cm^{-3}.

This lifetime difference arises from the high-injection level effect in the base of the high-resistivity cell and is also peculiar to the two-level Zn recombination model assumed.

The drop and minimum of the fill factor shown in Fig. 2 for the low-base-doping cell further illustrates the high-injection-level effect which pushes the diode characteristics from the ideal exp(qV/kT) law to the high-level exp(qV/2kT) law. The rise of FF at deeper BSF penetration comes from the increasing base doping and increasing base recombination due to Auger recombination in the BSF layer which reduces the photogenerated carrier density. Thus, both of these push the diode law towards the ideal law, thereby increasing the FF towards it ideal value determined by V_{OC} and $\exp(qV_{OC}/kT)$.

Due to the high injection level effect in the high-resistivity base layer, the efficiency increases continually with deeper penetrating BSF layer. Further penetration beyond 48 um will cause a rise of the total base doping and when that reaches 1.0E17, the efficiency would reach the 20% value of a 1.0E17 base-doping cell, such as that shown in Fig. 1.

From the above discussions, it is evident that both of these examples give one criterion which points to not only an extended BSF layer but also a high majority carrier or dopant impurity concentration, about 1.0E17, on the base side of the p/n junction, in order to reach the high open-circuit voltage or 20% AM1 efficiency.

III. IMMUNITY IMPROVEMENT TO THE PRESENCE OF RECOMBINATION CENTERS

One of the advantages offered by a deeply penetrating BSF layer is its increased immunity to higher densities of recombination centers, since the built-in drift field should aid the separation of electrons and holes, hence, lessen the probability that they recombine. This would improve not only the short-circuit current but also the minority carrier diffusion length in the base and hence the open-circuit voltage, in addition to that obtained from reduced recombination volume. Two series of cells are analyzed to provide quantitative estimates of the immunity improvement, expressed in terms of the recombination center density that can be tolerated at a given degradation rate. This rate is expressed as dZ/dNTT where Z is VOC, JSC, FF or EFF while NTT is the density of the recombination centers. The two families of curves obtained correspond to cells with a deeply penetrating BSF layer (40 um) and cells with a shallow or thin BSF layer (5 um). The latter is selected based on the results of Figs. 1 and 2 and also the recent production and research cell designs which have such a thin or even thinner BSF layers. The base dopant concentration of the p+/n/n+ cells is 1.0E17 and the total cell thickness is 50 um, all selected to give high VOC and high efficiency.

The results are shown in Fig. 3 for the thick BSF cells and in Fig.4 for the thin BSF cells.

It is evident that for the thick BSF cells shown in Fig. 3, the penetrating BSF has made the cell immune to recombination impurity densities up to about 1.0E12 cm^{-3}, the value we used in Figs. 1 and 2. A 2% efficiency drop from 20% to 18% occurs when the recombination impurity density is increased from 1.0E12 (20 us base lifetime) to

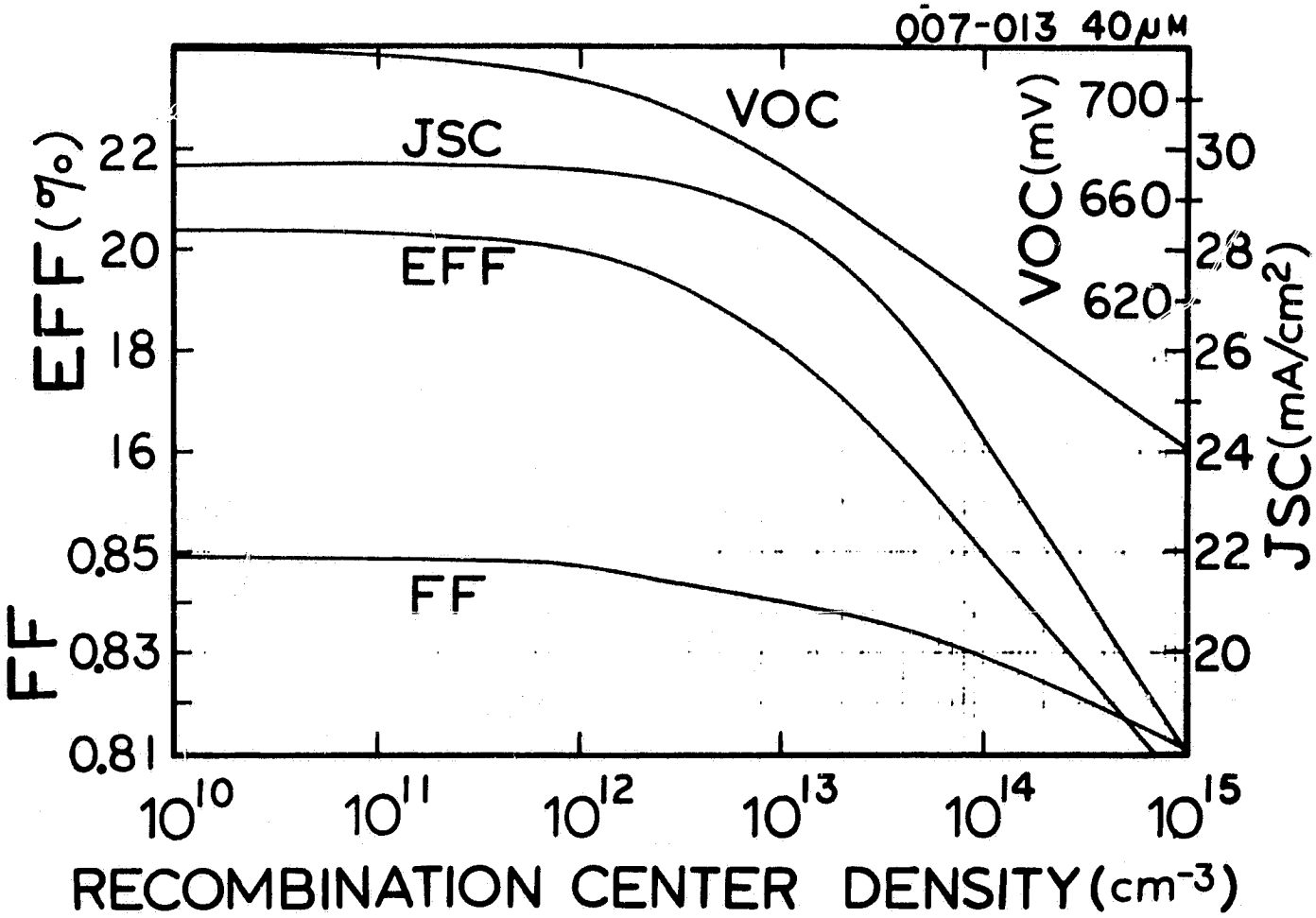

Fig. 3. Performance of p+/n/n+ silicon solar cells versus the density of recombination impurity with a base dopant density of 1.0E17 cm^{-3} and BSF penetration of 40 um.

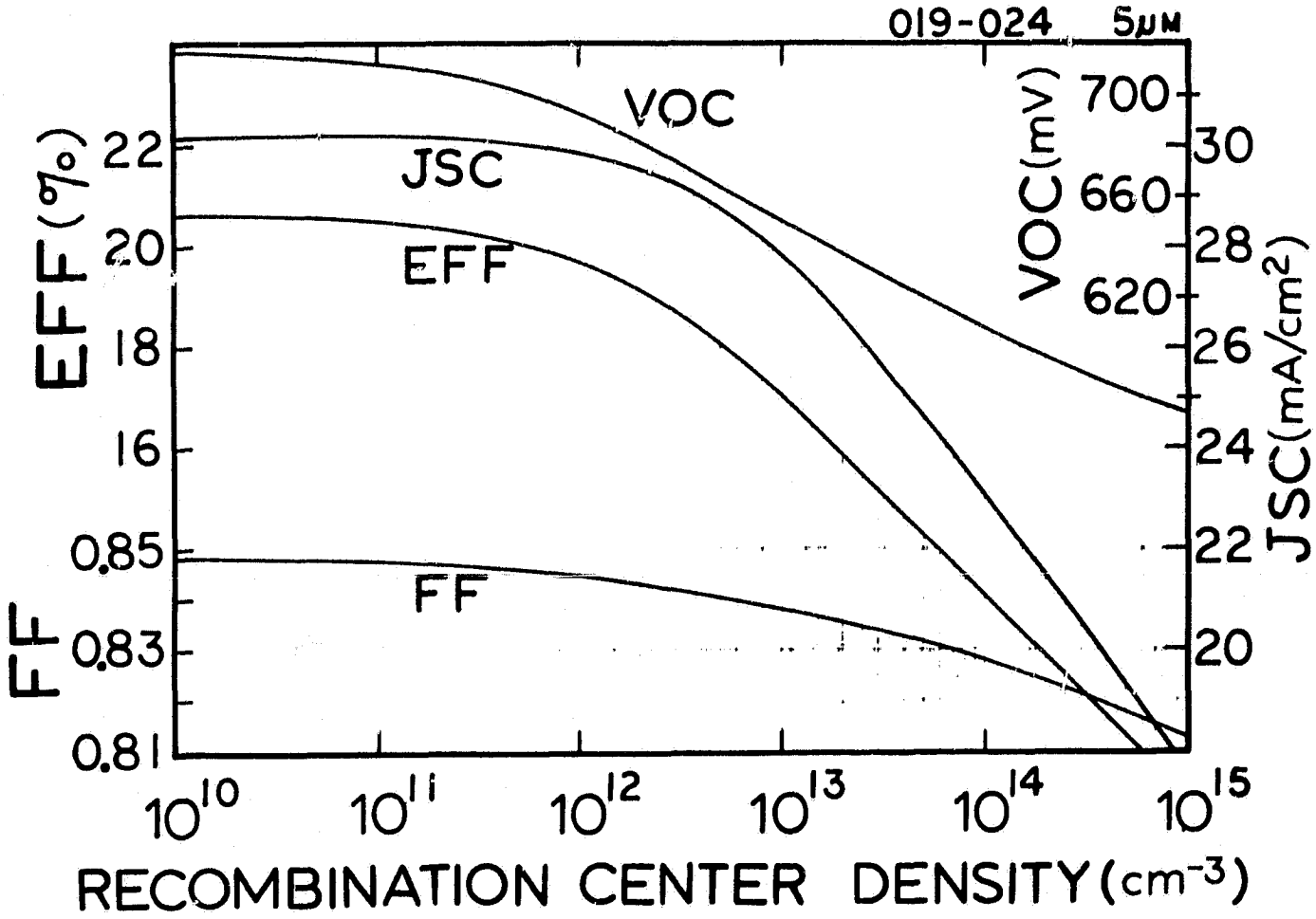

Fig. 4. Performance of p+/n/n+ silicon solar cells versus the density of recombination impurity with a base dopant density of 1.0E17 cm^{-3} and BSF penetration of 5 um.

1.0E13 cm^{-3} (2 us base lifetime). This comes about from reduction of both VOC and JSC.

On the other hand, the efficiency drop off of the non-penetrating BSF cells, shown in Fig. 4, begins at about 5.0E11. This is due mainly to the reduction of VOS since JSC is not affected until 1.0 to 2.0E11 recombination impurity densities is reached.

The above analyses show that a factor of two improvement in the immunity to recombination impurity density is obtained when the BSF layer is made to penetrate 40 um into a 50 um thick cell from a shallow penetration of 5 um.

The improvement factor for each of the four parameters can be individually estimated by sliding the corresponding curves from Fig. 3 and Fig. 4 along the horizontal axis (NTT) until the two corresponding curves nearly coincide at their maxima and their rapidly decreasing range. This graphical matching is equivalent to finding the NTT values at a constant dX/dNTT slope where X is one of the four parameters. From this graphical analysis, we obtain the following immunity improvement factors: VOC=3.5, JSC=2.5, FF=1.5 and EFF=2.5.

This procedure, if carried out for a whole range of penetration depth, will provide an universal scaling law for the prediction of the immunity tolerance of solar cells.

IV. COMPARISON OF p+/n/n+ AND n+/p/p+ CELLS

There are technological, performance as well as application reasons for using both the p+/n/n+ cells illustrated in the previous two sections and n+/p/p+ cells. For example, since electron mobility is nearly three times higher than hole mobility, one would expect higher performance from n+/p/p+ cells over similar structured p+/n/n+ cells, if base recombination is the limiting factor. On the other hand, if emitter recombination is limiting, such as the high efficiency cells in the efficiency saturation range (deep penetrating BSF layers in Figs. 1 and 2 and low recombination density range in Figs. 3 and 4), then one would expect higher performance from p+/n/n+ cells over n+/p/p+ cells instead. Additional and new exprimental evidence indicates that hole mobility in heavily doped n-type silicon, such as the diffused emitter in the n+/p/p+ cell, is extremely low [11] and limited by trapping at the shallow bandtail states near the valence band edge [12] which is sometimes known as hopping conduction. A similar but possibly lesser electron mobility reduction in heavily doped p-type silicon, such as the emitter of the p+/n/n+ cells, would also be expected. This would further emphasize the importance of emitter recombination as the limiting factor in high-efficiency cell designs. As an example of technological consideration, the p+/n/n+ extended BSF cell may be further favored by the well-known recombination-impurity-gettering property of the phosphorus diffused n+ layer during its formation at the diffusion temperature. This should further reduce the recombination center density in the p+ emitter and n-type base layers, thereby increasing the thermal recombination lifetimes in these layers. In contrast, the gettering action during the high-temperature formation of the diffused n+ emitter would increase the recombination impurity density

in the n+ emitter, reduce the emitter thermal recombination lifetime and hence decrease the short-circuit current and the limiting efficiency. A third and more fundamental consideration is that the interband Auger recombination rate in degenerate n-type silicon (2.8E-31 cm^6/s) is about three times larger than that in degenerate p-type silicon (0.99E-31 cm^6/s). This would also favor the p+/n/n+ over the n+/p/p+ high efficiency cells when emitter recombination is the limiting factor.

From the above three sample reasonings, one would expect the p+/n/n+ cells to have higher performance than the n+/p/p+ cells. To explore this difference in more quantitative detail and to demonstrate that interband Auger recombination in the emitter is the limiting mechanism of high-efficiency cell performance, the four performance parameters of four families of n+/p/p+ cells are computed using the CTSA program and the materials parameters described in section II. The four families consist of the two base dopings, 1.0E17 and 5.0E15, and two variations of the density profile of the phosphorus emitter. The net impurity density profiles are given by

$$N_{DD}-N_{AA} = C_0\exp[-(x/L_1)^6] - C_B - C_L\exp[-(L-x)/L_2] \quad \{\text{NORMAL}\} \quad (2)$$

$$N_{DD}-N_{AA} = C_0[1-(x/L_1)^{2/3}] - C_B - C_L\exp[-(L-x)/L_2] \quad \{\text{B-LIKE}\} \quad (3)$$

where C_0=5.0E20, C_B=1.0E17 or 5.0E15, C_L=5.0E18. L_1 is obtained from the assumed junction depth of 0.25 um, and L_2 is determined by the BSF penetration depth which assumes values of 1, 2, 5, 10, 20, 30, 40, 45, 48 and other intermediate values. The total cell thickness, L, is 50 um.

The two emitter profiles, employed to demonstrate the importance of interband Auger recombination in the emitter as the limiting mechanism, are labeled NORMAL, Eq.(2), and B-LIKE, Eq. (3). They are in the sense that the 'Normal' n+ profile in Eq. (2) is that normally observed after a high temperature phosphorus diffusion with a constant-surface-density phosphorus source, while the 'B-like' profile in Eq. (3) is the normally observed boron diffusion profile, although such a 'hypothetical' boron-like phosphorus diffusion profile can be readily obtained by epitaxial growth or ion implantation. The reason for using the B-like profile of Eq. (3) to represent the phosphorus diffusion in the n+ emitter of the n+/p/p+ cells is to pin-point the interband Auger recombination in the emitter as the source of different limiting performance between the p+/n/n+ and p+/n/n+ families, whose respective and identical net impurity concentration profiles are given by Eq. (1) and Eq. (3).

The performance parameters versus BSF penetration depth for the two 1.0E17 cm^{-3} base doping families of n+/p/p+ cells are shown in Fig. 5 (Normal) and Fig. 6 (B-like). The importance of interband Auger recombination in the emitter, which gives the p+/n/n+ family the higher performance, can now be demonstrated by overlaying the three families of curves of Figs. 1, 5 and 6. The following inequalities of the four parameters are observed. Here, GT means greater than, EQ means equal to, LT means less than, GE means greater than at deep BSF penetration and nearly equal to at shallow BSF penetration, and EG means equal to at shallow BSF penetration but greater than at deep BSF penetration.

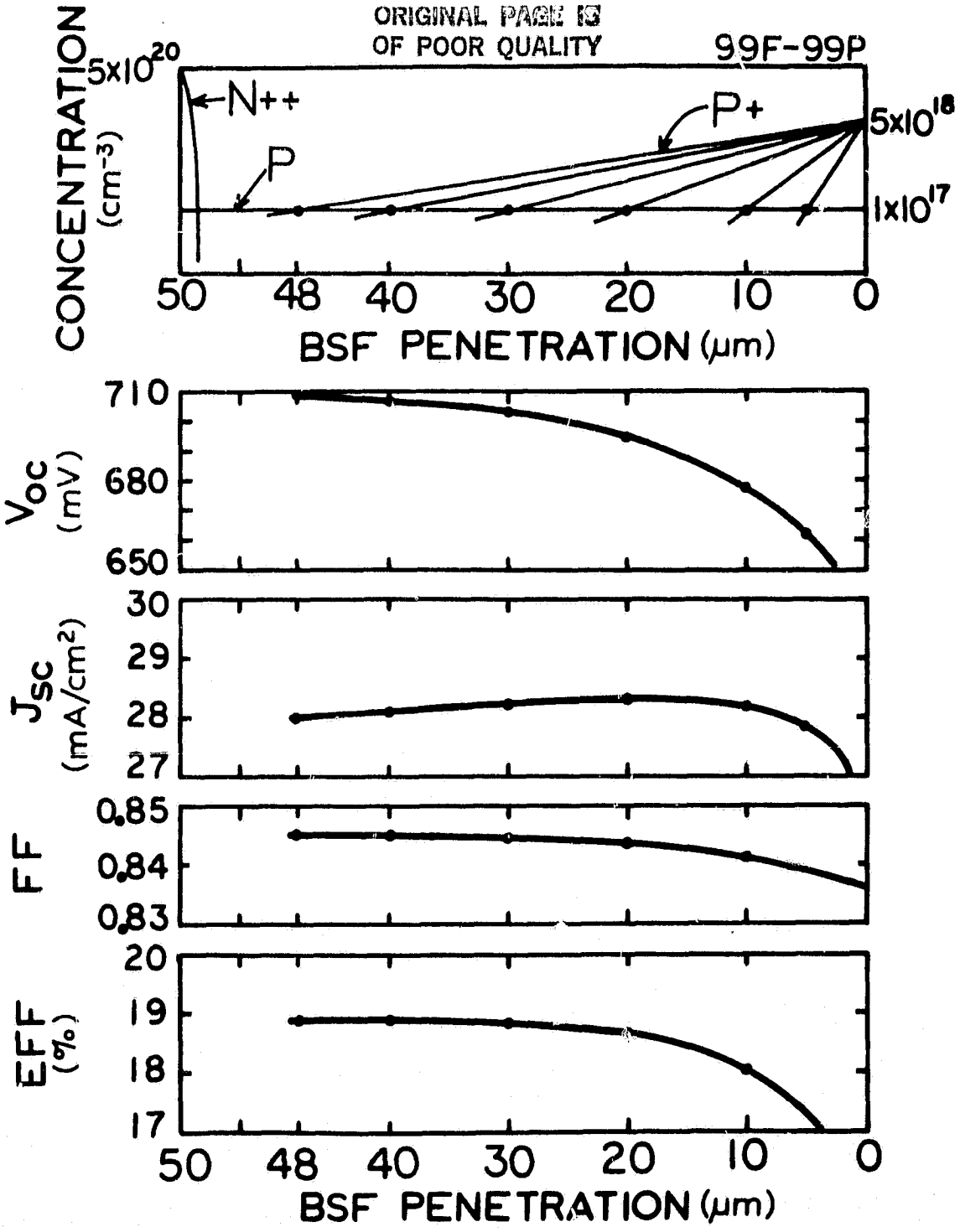

Fig. 5. Effect of BSF penetration on the performance of n+/p/p+ silicon solar cells with base dopant density of 1.0E17 cm^{-3} and a normal phosphorus diffusion profile in the emitter.

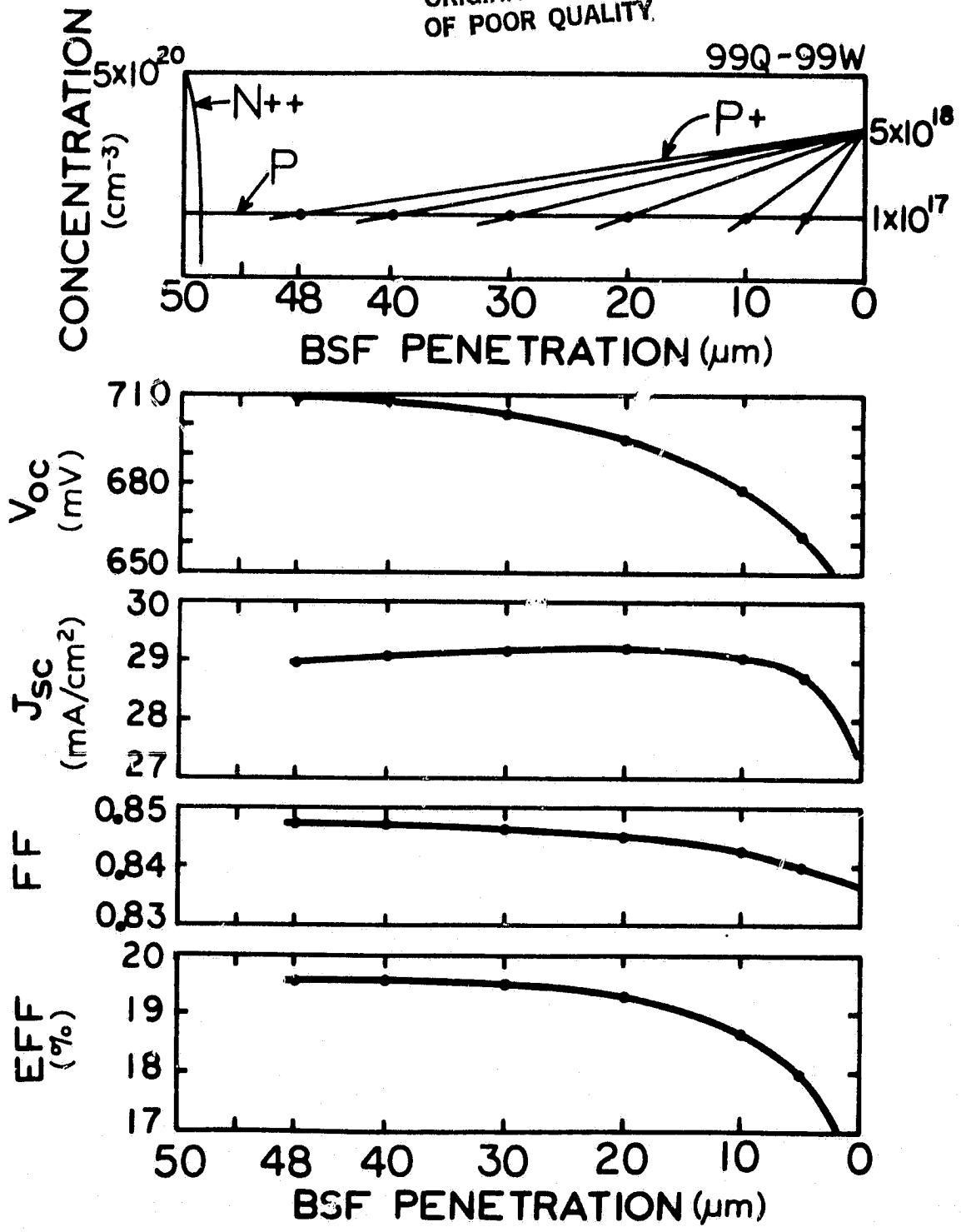

Fig. 6. Same as Fig. 5 but with a Boron-like phosphorus diffusion profile.

VOC p+/n/n+ EG n+/p/p+(B-like) EQ n+/p/p+(Normal) (4)

JSC p+/n/n+ GT n+/p/p+(B-like) GT n+/p/p+(Normal) (5)

FF p+/n/n+ EG n+/p/p+(B-like) GE n+/p/p+(Normal) (6)

EFF p+/n/n+ GT n+/p/p+(B-like) GT n+/p/p+(Normal) (7)

The higher performance of the n+/p/p+ cells with B-like phosphorus n+ emitter profile than that with the Normal phosphorus n+ emitter profile, as indicated by Eqs. (4) to (7), is a demonstration of the importance of interband Auger recombination in the emitter, since the normal phosphorus profile, $\exp(-x^6)$, gives a nearly constant electron concentration and hence constant and high Auger recombination rate over the entire emitter, while the B-like phosphorus profile, $1-x^{2/3}$, gives a rather graded impurity and electron concentration profile that decreases to fairly low values as one approaches the emitter side of the junction-space-charge-layer boundary. This lower electron density results in lower hole recombination rate via the interband Auger mechanism which is given by $c_p^n N^2$.

A similar consideration can be made to show that the lower interband Auger recombination rate in the emitter of the p+/n/n+ cell gives its higher performance than the n+/p/p+ cells, as indicated by Eqs.(4) to (7). In particular, the built-in electric field in the emitter is not the deciding factor since the B-like-emitter n+/p/p+ cells, Eq. (3), have exactly the same built-in electric field variation in its emitter layer as the p+/n/n+ cells, Eq. (1). The difference is due to

the higher lifetime in the p+ emitter than in the n+ emitter or the lower interband Auger recombination rate of the electrons in the p+ emitter than the holes in the n+ emitter, as discussed earlier.

V. LOCAL STEADY-STATE LIFETIMES

The interband Auger recombination mechanism that gives performance advantage to the p+/n/n+ cells over the n+/p/p+ cells is further demonstrated by an illustration of the position variations of the 'local' steady-state lifetimes in the three families of cells at the 1.0E17 base doping, shown in Figs. 1, 5 and 6. The local steady-state lifetime is defined in the usual Shockley-Read-Hall sense who intended to provide a linearized appearance to the minority carrier diffusion equations so that they can be solved analytically. Their mathematical definitions are used in our numerical analysis which are

$$TN = [N(x) - NE(x)]/RN(x) \qquad \text{electrons} \qquad (8)$$

and

$$TP = [P(x) - PE(x)]/RP(x) \qquad \text{holes} \qquad (9)$$

TN and TP are the local steady-state lifetimes, N(x) and P(x) the steady-state densities, NE(x) and PE(x) the equilibrium densities, and RN(x) and RP(x) the total steady-state recombination rates of electrons and holes respectively at location x. RN and RP are the sums of the interband Auger and band-bound localized thermal recombination rates.

The depth variations of the local steady-state lifetimes in the low-base-resistivity cell of 1.0E17 base doping, with a BSF penetration of 20 um given in Fig. 1, are shown in Fig. 7. The + labels are for holes and the - labels are for electrons. There are three figures in Fig. 7. The upper, middle and lower figures correspond respectively to the three

OF POOR QUALITY

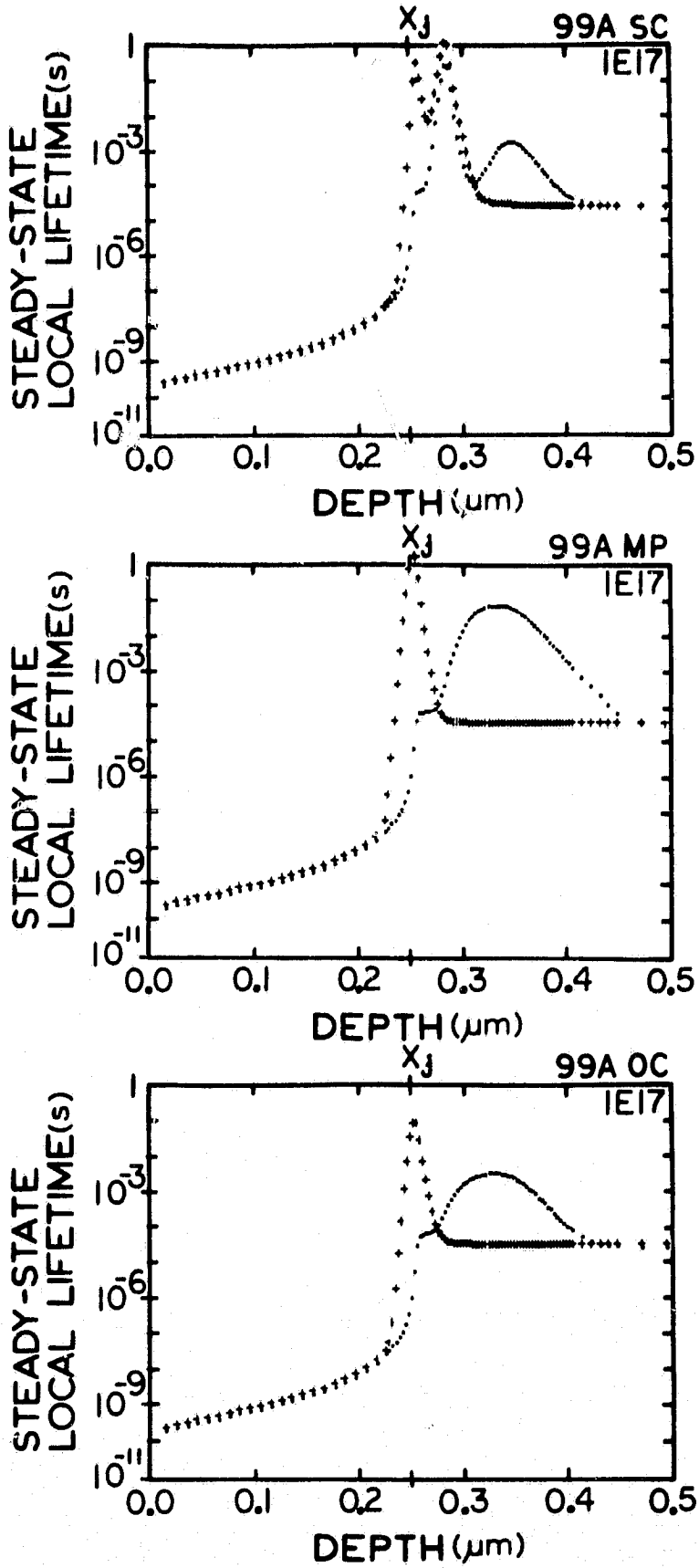

Fig. 7 Spatial (depth) variation of the local steady-state lifetimes of the p+/n/n+ cell of 20 um BSF penetration and 1.0E17 base doping at the three load conditions, OC=Open-Circuit, MP=Maximum-Power and SC=Short-Circuit.

load conditions, the short-circuit (SC), the maximum-power (MP), and the open-circuit (OC) conditions.

The position range covers the quasi-neutral emitter layer from 0 to 0.22 um, the space-charge layer from 0.22 to 0.45 um, and a thin top layer of the quasi-neutral base from 0.45 to 0.50 um.

The main features in these three figures in Fig. 7 is that the local steady-state lifetimes in the space charge layer are rather useless quantities due to their wild variations with positions, an observation also made previously by us [13]. However, the curves show that the lifetimes in the quasi-neutral emitter and base regions are well-behaved and predictable from simple analytical approximations.

To demonstrate the importance of interband Auger recombination in the quasi-neutral emitter layer on limiting the cell performance at high efficiency, the local lifetimes of the three low-base-resistivity cells with 1.0E17 cm^{-3} base doping and 20 um BSF penetration, given in Fig. 1 (p+/n/n+), Fig. 5 (n+/p/p+ Normal), and Fig. 6 (n+/p/p+ B-like), are presented together in Fig. 8.

The emitter is at low injection level under all SC, MP, and OC conditions so that all the six lifetimes (minority and majority carriers at the three load conditions) are nearly equal. Hence, they are shown as a single curve for each cell in Fig. 8.

The curves in Fig. 8 are lifetimes of the combined interband Auger and localized thermal recombination mechanisms as defined by Eqs.(8) and (9). RN and RP are the sums of the rates of these two mechanisms. However, in the diffused emitter, the Auger rate (1 to 100 ps lifetime) is much faster than the thermal rate at recombination centers (1 to 100 us). Thus, the combined lifetime in the quasi-neutral emitter is essentially that of Auger lifetime.

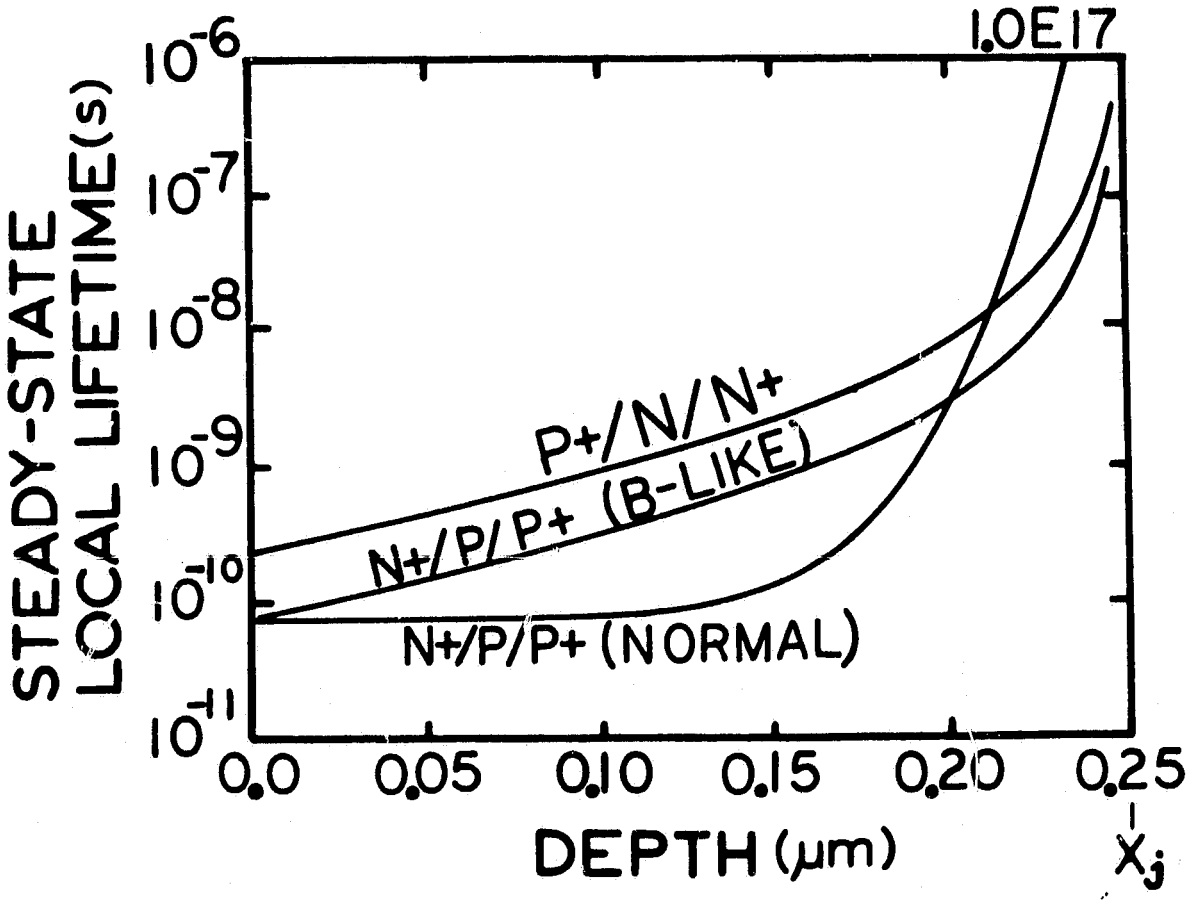

Fig. 8. Spatial variation of the local steady-state lifetimes at the Maximum-Power load in the p+/n/n+ and two n+/p/p+ cells of 20 um BSF penetration and 1.0E17 base doping.

The results presented in Fig. 8 indicate that the emitter lifetimes of the three 1.0E17 base-doping cells follow the inequality observed for the short-circuit current and efficiency which were given in Eqs. (5) and (7). This correlation is a direct indication that the emitter recombination is limiting the performance of high efficiency silicon solar cells whose localized thermal recombination rates in the base and emitter regions have been reduced to insignificant levels.

The comparisons just presented using Figs. 1, 5, 6, 7 and 8 are for the low-base-resistivity cells with 1.0E17 cm^{-3} base dopant impurity concentration. A similar comparison has also been made for the high-base-resistivity cells with 5.0E15 cm^{-3} base dopant impurity concentration. The conclusions drawn above are also applicable for the high-base-resistivity cells. The set of figures, corresponding to Figs. 5-8, are given in Figs. 9-12, without further elaboration. These figures are included here not just for completeness but for the fact that most of the current high-efficiency silicon solar cells at the 15 to 17% AM1 efficiency range, under development or engineering tests, are high-base-resistivity cells. Thus, Figs. 9-12 would be particularly valuable to illustrate the basic physical mechanisms in currently available cells and to point to the performance improvement and limitation one could expect when the resistivity is lowered or the base dopant impurity concentration is increased to 1.0E17 cm^{-3}.

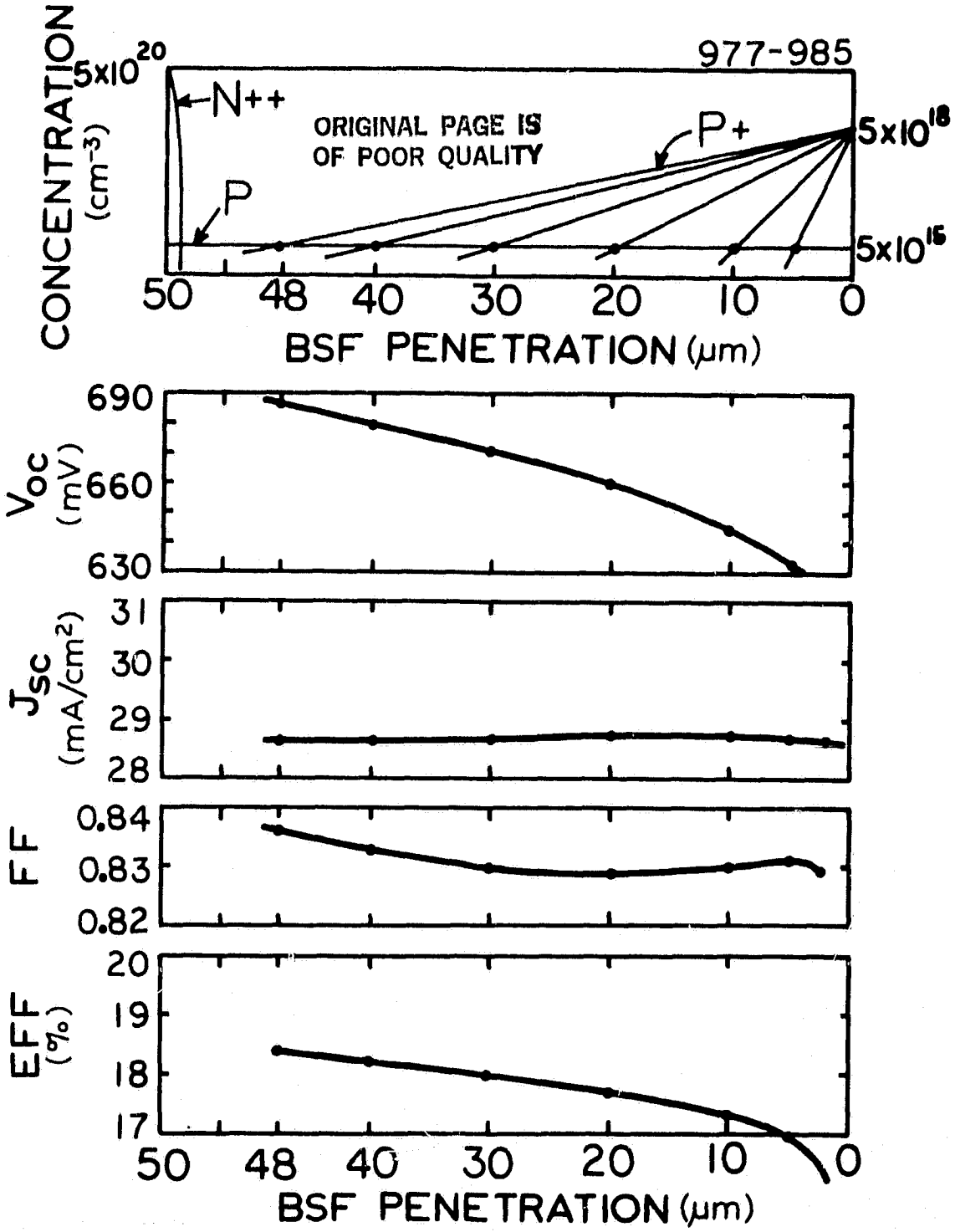

Fig. 9. Similar to Fig. 5 but for a base doping of 5.0E15 cm^{-3}.

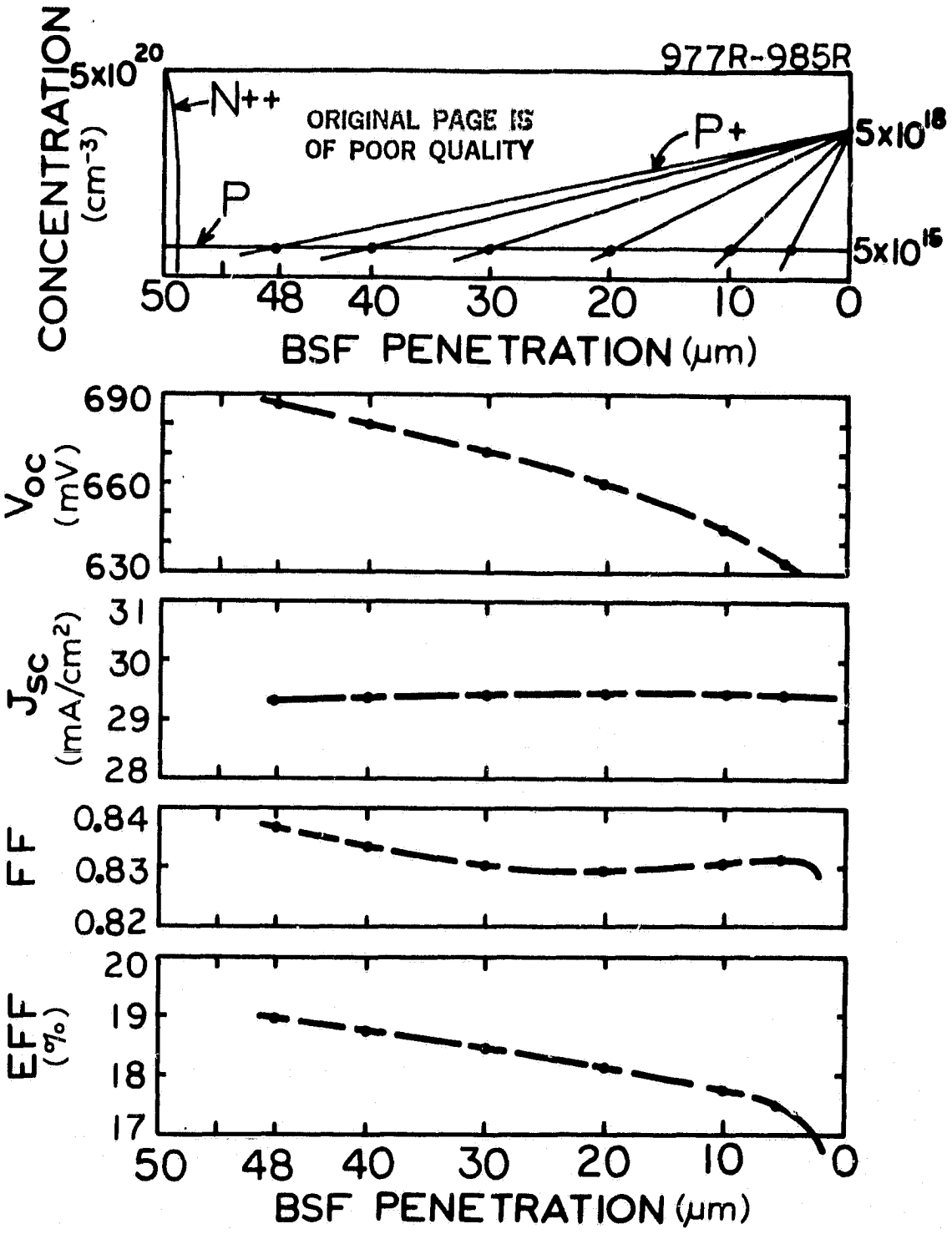

Fig. 10. Similar to Fig. 6 but for a base doping of 5.0E15 cm^{-3}.

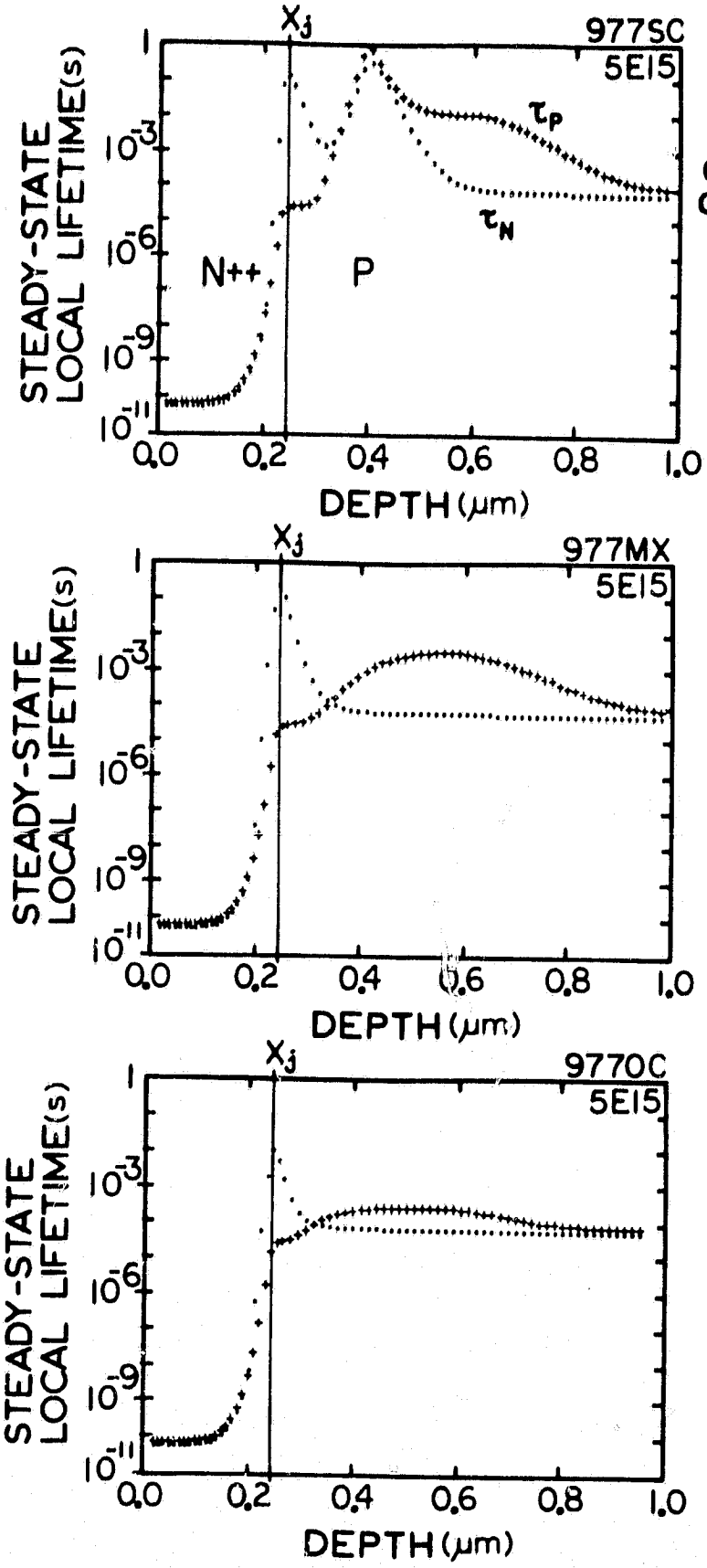

Fig. 11. Similar to Fig. 7 but for a base doping of 5.0E15 cm^{-3}.

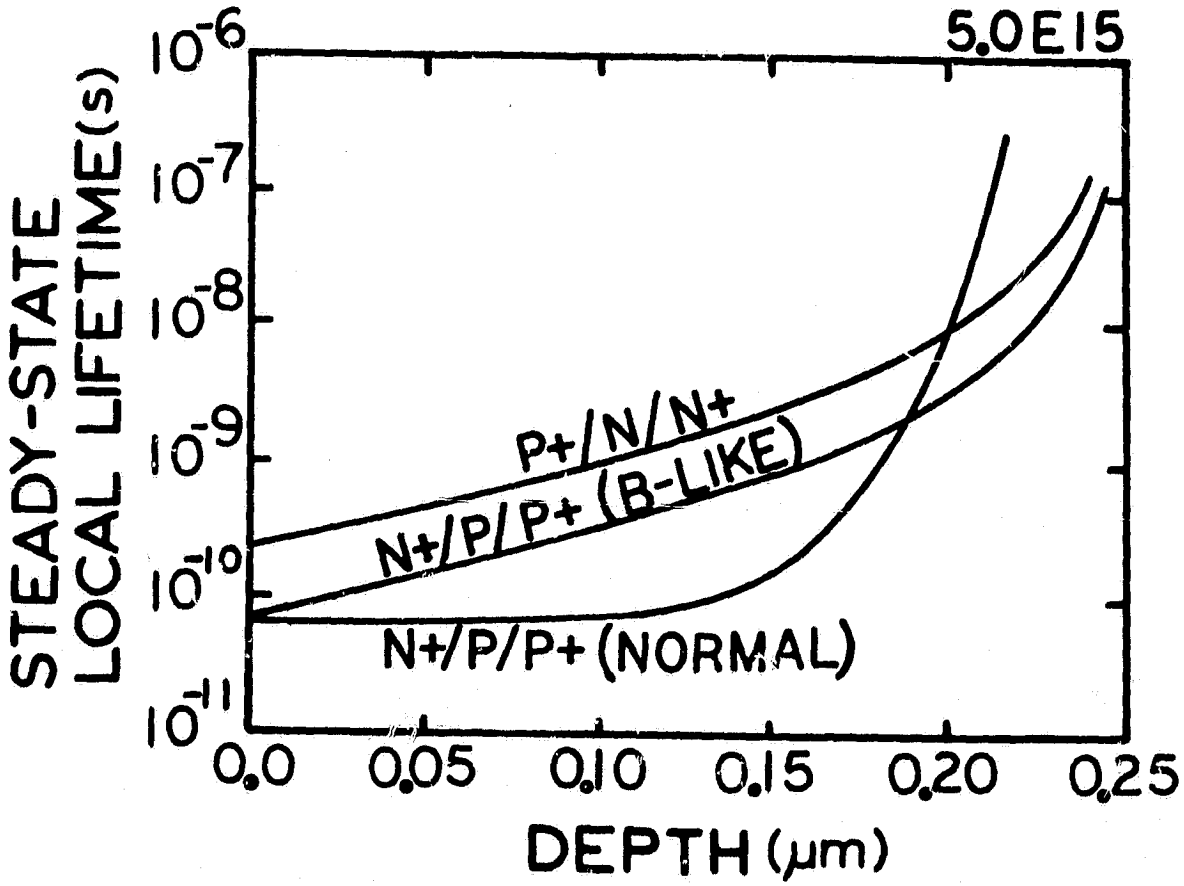

Fig. 12. Similar to Fig. 8 but for a base doping of 5.0E15 cm^{-3}.

VI. CONCLUSION AND SUMMARY

The analyses presented in this paper provide the following indicators of the physical mechanisms which limit the performance of the solar cell. (1) The extended back-surface-field layer will improve the open-circuit voltage significantly. It is a result of reducing the volume of localized recombination of electrons and holes at the recombination impurity and defect centers in the bulk of the silicon substrate. For the optimum thickness cell of 50 um thick, a BSF penetration of 20 um with a density of 5.0E18 cm^{-3} on the back surface is sufficient to give nearly the limiting open-circuit voltage (710 mV) and limiting efficiency (20%). (2) There is no significant difference between the p-base and n-base extended BSF cells due to the different electron and hole mobilities, as suggested in the past. This lack of difference in the high efficiency cells comes from the fact that the limiting factor is no longer due to recombination in the base, but in the emitter. (3) In high-efficiency cells with the extended BSF layers, emitter recombination becomes the limiting factor on the highest achievable efficiency. The ultimate limit comes from the 'unavoidable' interband Auger recombination of electrons and holes in the high-concentration emitter. The p+ emitter in the p+/n/n+ cell structures has a higher lifetime and hence gives a higher short-circuit current than the n+ emitter in the n+/p/p+ cell structures. This comes about because the interband Auger recombination rate of electrons in heavily doped p+ emitter is smaller than that of holes in heavily doped n+ emitter. If the current accepted numerical values of these Auger recombination rates are revised by new measurements, then a similar revision of this conclusion must be made. (4) Proper design or variation, by ion implantation or epitaxial growth,

of the emitter impurity or majority concentration profile can reduce the interband Auger recombination rate substantially. However, multi-parameter optimization is required to take into account of the emitter surface recombination and series resistance effects which become important when the emitter dopant concentration is reduced and both effects reduce efficiency. (5) When emitter recombination is the limiting factor, the limitation is on the short-circuit current and not on the open-circuit voltage as suggested in the past. As much as 10% or more in short-circuit improvement may be obtained by reducing the emitter dopant impurity concentration near the edge of the junction space-charge layer.

VII. ACKNOWLEDGEMENT

This work is supported by the U. S. Department of Energy through the Jet Propulsion Laboratory. We would like to thank our former and current technical monitors, Drs. K. Alan Yamakawa, Ralph Lutwack and Li-Jen Cheng. We are also indebted to Professor Fred A. Lindholm for continued exchange of information, discussion and collaboration.

VIII. REFERENCES

1. Michael P. Godlewski, Cosmo R. Baraona and Henry W. Brandhorst, Jr. "Low-High Junction Theory Applied to Solar Cells," Conference Record of 10th IEEE Photovoltaic Specialist Conference, pp. 40-49, IEEE Catalog No. 73CH0801-ED (1973).

2. J. G. Fossum and E. L. Burgess, "High Efficiency p+/n/n+ Back-Surface-Field Silicon Solar Cells," Applied Physics Letters, 33, pp. 238-240 (1978); J. G. Fossum, R. D. Nasby and E. L. Burgess, "Development of High-Efficiency p+/n/n+ Back-Surface-Field Silicon Solar Cells," Conference Record of 13th IEEE Photovoltaic Specialist Conference, pp. 1294-1299 (1978). IEEE Catalog No. 78CH1319-3.

3. C. T. Sah, K. A. Yamakawa and R. Lutwack, "Reduction of Solar Cell Efficiency by Edge Defects Across the Back-Surface-Field Junction:- A Developed Perimeter Model," Solid-State Electronics, 25, pp. 851-858 (1982).

4. C. T. Sah, K. A. Yamakawa and R. Lutwack, "Reduction of Solar Cell Efficiency by Bulk Defects Across the Back-Surface-Field Junction," Journal of Applied Physics, 53(4), pp.3278-3290 (1982)

5. H. W. Brandhorst, Jr. "Current Status of Silicon Solar Cell Technology," Presented at the 1975 International Electron Device Meeting, Paper 15.1, Washington, D.C. Technical Digest of IEDM-75, IEEE, N.Y.

6. F. A. Lindholm, A. Neugroschel, C. T. Sah, M. P. Godlewski and H. W. Brandhorst, Jr., "Methodology for the experimental determination of the gap shrinkage and lifetimes in the emitter and base of p-n junction solar cells and other p-n junction devices," IEEE Transaction on Electron Devices, ED-36(4), pp.402-410 (1977).

7. F. A. Lindholm and C. T. Sah, "Fundamental Electronic Mechanisms Limiting the Performance of Solar Cells," IEEE Transaction on Electron Devices, ED-24(4), pp.299-304 (1977).

8. A. Meulenberg, Jr. "Development Toward an 18% Efficient Silicon Solar Cell," Final Report, Contract NAS-3-22217, April 1983, COMSAT Laboratories, Clarksburg, MD 20871; A. Meulenberg and R. A. Arndt, "Limitations on Solar Cell Open-Circuit Voltage and Efficiency," COMSAT Technical Review, Vol. 14, Spring 1983.

9. Chih-Tang Sah, K. Alan Yamakawa and Ralph Lutwack, "Effect of Thickness on Silicon Solar Cell Efficiency," IEEE Transaction on Electron Devices, Vol. ED-29(5), pp.903-908 (1982).

10. Chih-Tang Sah, Phillip Ching-Ho Chan, Alex Chi-Kuo Wang, Robert L. Y. Sah, K. Alan Yamakawa and Ralph Lutwack, "Effect of Zinc Impurity on Silicon Solar Cell Efficiency," IEEE Transaction on Electron Devices, Vol. ED-28(3), pp.304-313(1981).

11. A. Neugroschel, F. A. Lindholm and C. T. Sah, "Measured Energy-Gap Narrowing and Effective Mass in n+ Si with Implications About Minority-Carrier Transport," Applied Physics Letters, Submitted.

12. C. T. Sah and F. A. Lindholm, "Transport in Semiconductors with Low Scattering Rate and at High Frequencies," Solid-State Electronics, Vol. 16(12), pp.1447-1448 (1973).

13. C. T. Sah, "Study of the Effects of Impurities on the Properties of Silicon Materials and Performance of Silicon Solar Cell," First Technical Report, pp.68-70, April 1978, DOE/JPL 954685-78/1.